

Specific selection on *XEG1* and *XLP1* genes correlates with host range and adaptability in *Phytophthora*

Received: 15 July 2024

Accepted: 28 March 2025

Published online: 17 April 2025



Qi Zhang^{1,2}, Xi Chen^{1,2}, Haixia You^{1,2}, Bing Chen^{1,2}, Liyu Jia^{1,2}, Sizhe Li^{1,2}, Xinyu Zhang^{1,2}, Ji Ma^{1,2}, Xinyi Wu^{1,2}, Kaixiang Wang^{1,2}, Huanshan Liu^{1,2}, Haibin Jiang^{1,2}, Junhua Xiao^{1,2}, Haidong Shu^{1,2}, Zhichao Zhang^{1,2}, Min Qiu^{1,2}, Ye qiang Xia^{1,2}, Han Chen^{1,2}, Yan Wang^{1,2}, Wenwu Ye^{1,2}, Suomeng Dong^{1,2}, Zhenchuan Ma^{1,2,3,4}✉ & Yuanchao Wang^{1,2,3,4}✉

In diverse *Phytophthora*-plant pathosystems, *Phytophthora* secretes XLP1 (PsXEG1-Like Protein), a non-enzymatic paralog that functions as a decoy to protect XEG1 (Xyloglucan-specific Endoglucanase) from host inhibitors. Here, we show that the genus-specific selection pressures on the *XEG1/XLP1* gene pair are crucial for host adaptation and are closely linked to *Phytophthora* host range. Our findings reveal that the *XEG1/XLP1* gene pair originated within *Phytophthora* and subsequently evolved into genus-specific genes, undergoing functional divergence driven by preferential selection. Positive selection sites within the *XEG1/XLP1* gene pair in *Phytophthora* contribute to this functional divergence and are associated with the host range variability of *Phytophthora* as evidenced by multivariate statistical analyses. Furthermore, mutations at key selection sites in *Phytophthora sojae* and *Phytophthora capsici* significantly impair their pathogenicity, with *P. capsici* exhibiting almost no colonization expansion on tobacco and pea. Notably, natural *Phytophthora* populations harbor mutations at the positive selection sites, indicating ongoing evolutionary pressures on the *XEG1/XLP1* gene pair.

Phytophthora, which diverged about 70 million years ago, belongs to oomycetes, a group that looks similar to filamentous fungi but is classified as *Stramenopiles*, which includes diatoms and brown algae^{1–4}. The most notorious species is *Phytophthora infestans*, which caused the potato famine in the 1840s⁵. The *Phytophthora* genus consists of 180 known species that infect a wide variety of plants in both managed and natural ecosystems, including crops, trees, and ornamentals^{6,7}. The host ranges of *Phytophthora* species vary from 1 to 327 host species⁸.

Apoplastic and cytoplasmic effectors have evolved to facilitate parasitism by suppressing plant immunity and altering plant physiology to promote the growth and spread of parasites^{9,10}. The apoplastic

effectors in *Phytophthora* are intricately linked to their host range, and there is a notable correlation between apoplastic effector abundance and the breadth of host species⁸. Apoplastic effectors in *Phytophthora* encompass various proteins, such as glycoside hydrolases, protease inhibitors, necrosis-inducing proteins (NLPs), proteases, lipases, and lipid-binding proteins. Among them, glycoside hydrolases are predominant within the suite of apoplastic effectors⁸.

Glycoside hydrolase 12 (GH12) family proteins, such as XEG1, are present in *Phytophthora* species and are thought to have originated through horizontal gene transfer from fungi¹¹. *P. sojae* XEG1 (PsXEG1) exhibits xyloglucan-hydrolyzing activity and plays a crucial role in virulence by degrading plant cell wall components¹². However,

¹Department of Plant Pathology, Nanjing Agricultural University, Nanjing 210095, China. ²Key Laboratory of Soybean Disease and Pest Control (Ministry of Agriculture and Rural Affairs), Nanjing Agricultural University, Nanjing 210095, China. ³Zhongshan Biological Breeding Laboratory, Nanjing 210095, China.

⁴These authors contributed equally: Zhenchuan Ma, Yuanchao Wang. ✉e-mail: zhenchuan.ma@njau.edu.cn; wangyc@njau.edu.cn

soybean counters this attack by producing an apoplastic glucanase inhibitor protein, GmGIP1, which binds to PsXEG1 and blocks its contribution to virulence. To evade this defense, *P. sojae* secretes a paralogous protein, PsXLP1, which lacks enzymatic activity but binds GmGIP1 with higher affinity than PsXEG1. This competitive binding effectively liberates PsXEG1, allowing it to facilitate infection¹³. In addition to GmGIP1, soybean employs a second layer of defense by secreting an aspartic protease, GmAP5, into the apoplast. GmAP5 binds to and degrades PsXEG1, thereby diminishing its virulence¹⁴. Remarkably, N-glycosylation of PsXEG1 provides two advantages: it shields the protein from degradation by GmAP5 and reduces its inhibition by GmGIP1¹⁴, enhancing PsXEG1's effectiveness in supporting *P. sojae* infection. Moreover, PsXEG1 functions as a pathogen-associated molecular pattern (PAMP) that is recognized by the host, triggering PAMP-triggered immunity (PTI) and inducing cell death in soybean¹². However, during natural infections, PTI responses elicited by PsXEG1 are actively suppressed by pathogen-derived effectors, such as RXLR effectors¹⁵. The pivotal apoplastic effector XEG1 and its paralog XLP1 constitute a focal point of coevolutionary struggle between *P. sojae* and soybean. Additionally, the gene pair encoding *PsXEG1* and *PsXLP1* is conserved in many *Phytophthora* species, highlighting the crucial role of the *XEG1/XLP1* gene pair in the biology and adaptation of *Phytophthora* species.

Here, evolutionary analyses reveal that the *XEG1/XLP1* gene pair originated within the *Phytophthora* genus and evolved into a genus-specific gene pair. The functions of XEG1/XLP1 have diverged significantly among *Phytophthora* species, particularly in inducing cell death, triggering defense gene expression, and producing reducing sugars in *Nicotiana benthamiana*. Ancestral genes reconstruction and replacement experiments in *P. sojae* provide strong evidence of functional divergence, highlighting evolutionary shifts from ancestral to modern sequences. Fourteen positive selection sites were identified in XEG1/XLP1, with no correlation to general genotypic relationships in *P. capsici*. Bidirectional mutational experiments between ancestral and modern sequences confirmed the role of positive selection pressure in driving functional divergence. Multivariate analyses further revealed a strong correlation between XEG1/XLP1 divergence and host range diversity, with three key positive selection sites identified. In *P. capsici*, mutations at a key positive selection site were validated through inoculation experiments on fourteen plant species, revealing that the positive selection site impacts infection capabilities on five plant species. Notably, *P. capsici* exhibited almost no colonization expansion on tobacco and pea. Selection pressure sites were also detected in natural *Phytophthora* populations, emphasizing their evolutionary significance. In *P. sojae*, mutations reverting XEG1/XLP1 to ancestral forms at positive selection sites indicated that they enhance host adaptability. Additionally, two natural mutations at positive selection pressure site 62 were validated as critical for *P. sojae* host adaptation. Together, these findings highlight that genus-specific selection pressures on XEG1/XLP1 are essential for host adaptation and closely linked to host range diversity in *Phytophthora*.

Results

Origin and functional divergence of the *XEG1/XLP1* gene pair in *Phytophthora*

To study the distribution of GH12 family proteins, we analyzed 66 oomycete species spanning multiple genera, including *Albugo*, *Aphanomyces*, *Bremia*, *Hyaloperonospora*, *Nothophytophthora*, *Peronospora*, *Peronosclerospora*, *Phytophthora*, *Phytophthium*, *Pilaspangium*, *Plasmopara*, *Pythium*, and *Saprolegnia*. Most of these species are recognized as plant pathogens, while *Saprolegnia*, *Aphanomyces*, and some species of *Pythium*, such as *Pythium insidiosum*, are known to infect animals or humans (Supplementary Data 1 and 2). The majority of GH12 protein sequences were only identified in plant pathogens, including *Phytophthora*, *Bremia*, *Peronospora*,

Peronosclerospora, and *Hyaloperonospora*, with *Phytophthora* exhibiting the highest abundance (Fig. 1a). To investigate the evolution of these GH12 family proteins, we constructed a phylogenetic tree utilizing all the GH12 family proteins found in oomycetes and those previously identified in fungi and bacteria¹². The result revealed that GH12 proteins from fungi and bacteria form distinct branches, separate from GH12 proteins of oomycetes. Within oomycetes, the GH12 proteins grouped into four distinct clades (Supplementary Fig. 1), exhibiting both quantitative expansion and evolutionary diversity. Notably, the orthologs of PsXEG1 and PsXLP1 formed independent subclades and exhibited later evolutionary divergence compared with other GH12 proteins of oomycetes (Fig. 1b and Supplementary Fig. 1). Both subclades contain 41 *Phytophthora* species, and only *P. pinifolia* and *P. hibernalis* are missing due to low-quality sequencing assemblies.

To further understand the evolutionary dynamics of these subclades, we conducted purifying selection analysis using two datasets. The first focused on the GH12 proteins from *Phytophthora* (Fig. 1c), and the second incorporated GH12 proteins from bacteria, fungi, and oomycetes (Supplementary Fig. 2a). Both PsXEG1 and PsXLP1 subclades showed evidence of purifying selection, as indicated by nonsynonymous-to-synonymous substitution rate ratios (ω) below 1 in both datasets (Fig. 1c and Supplementary Fig. 2a). In addition, both subclades also exhibited a distinct conservative pattern (Supplementary Fig. 2b).

To determine whether the genes within the PsXEG1 and PsXLP1 subclades are *XEG1* and *XLP1* genes in the corresponding *Phytophthora* species, we performed a detailed scan of the *Phytophthora* genomes to identify adjacent upstream and downstream genes, followed by collinearity analysis (Supplementary Data 3). The analysis confirmed that the genes within the PsXEG1 and PsXLP1 subclades are indeed orthologous to XEG1 or XLP1 in the respective *Phytophthora* species, suggesting that the *XEG1/XLP1* gene pair originated within *Phytophthora*. Given that *PsXEG1* and *PsXLP1* in *P. sojae* are arranged in a head-to-head configuration within the genome, we focused on orthologs exhibiting this arrangement for further analysis, encompassing 26 *Phytophthora* species (Supplementary Fig. 2c, d).

To investigate the functional differences of XEG1 and XLP1 across various *Phytophthora* species, we evaluated their abilities to induce cell death, trigger defense gene expression, and produce reducing sugars in *N. benthamiana* using *Agrobacterium*-mediated transient expression. For the assessment of cell death induction, we measured electrolyte leakage as an indicator of cell death intensity induced by XEG1 and XLP1 orthologs. *P. palmivora* was excluded due to unsuccessful gene synthesis. Except for *P. idaei* XLP1, all tested PsXEG1 and PsXLP1 orthologs elicited varying degrees of cell death compared to the empty vector control with GFP (Supplementary Fig. 3a). To evaluate their ability to trigger defense responses, we examined the expression of defense genes related to PTI, salicylic acid (SA), ethylene (ET), and jasmonic acid (JA) at 12-, 24-, and 36-h post-infiltration. Most defense genes were induced by XEG1 or XLP1 at 24 h, with *Acre31*, *CYP71D20*, *PAL10*, *AOS*, and *Pti5* showing stronger induction than *WRKY8* (Supplementary Fig. 4). For the capacity to generate reducing sugars, we measured the apoplastic reducing sugar levels in *N. benthamiana* expressing the corresponding XEG1 or XLP1 (Supplementary Fig. 5a). In 18 species, XEG1 orthologs exhibited higher reducing sugar production compared to their respective XLP1. In contrast, XLP1 orthologs exhibited higher activity in four species (*Phytophthora europaea*, *Phytophthora chlamydospora*, *Phytophthora parvispora*, and *Phytophthora pseudosyringae*) and similar activity to XEG1 in two species (*Phytophthora aleatoria* and *Phytophthora idaei*) (Supplementary Fig. 5b, c). These proteins were effectively expressed at the expected size in *N. benthamiana*, as confirmed using western blot analysis (Supplementary Fig. 3b). A comprehensive analysis of both XEG1 and XLP1 revealed that XEG1 led to higher levels of defense response genes and reducing sugars compared to XLP1, although there were no

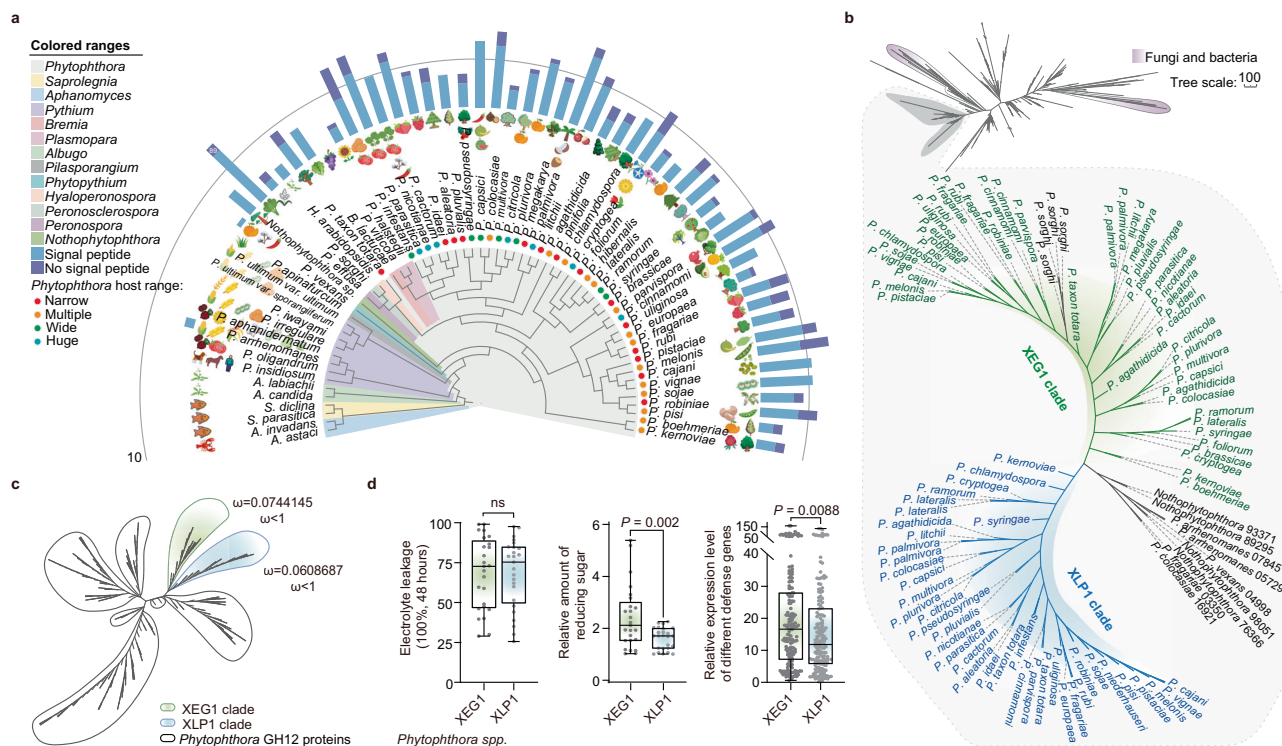


Fig. 1 | Phylogenetic distribution and functional characterization of PsXEG1 and its paralog PsXLP1 in relation to their orthologs across *Phytophthora* clades. **a** Distribution and quantity of GH12 family proteins in oomycetes infecting plants and animals. Distinct genera are represented by distinct colors. The outer circle indicates the quantity of the presence and absence of signal peptides in GH12 family proteins across various oomycetes, while the inner circle represents the host range diversity of *Phytophthora* pathogens, with four colors denoting distinct host ranges. The number of homologous proteins without signal peptides of *Peronospora effusa* is indicated by numbers. Icons depict representative host plants or animals infected by these pathogens. **b** Phylogenetic tree of GH12 family proteins across oomycetes, fungi, and bacteria. The phylogeny was constructed using sequences from selected species within these groups. Subclades containing PsXEG1 and PsXLP1 are highlighted, showing that these proteins form a well-supported clade within the *Phytophthora* genus. Detailed protein information and phylogenetic tree data are available in Supplementary Data 1, 2 and Source Data. **c** Evolutionary analysis of the XEG1/XLP1 subclades. The purifying selection rates (ω) for each clade were estimated based on the nonsynonymous to synonymous ratio

($\omega < 1$), indicating purifying selection. **d** Phenotypic characterization of *Phytophthora* XEG1 and XLP1 in *Nicotiana benthamiana*. Multiple phenotypic assays were conducted to evaluate the functional effects of XEG1 and XLP1 in different *Phytophthora* species in *Nicotiana benthamiana*. Electrolyte leakage, indicative of cell death, was quantified 48 h post-infiltration. Each point represents the average of nine biological replicates ($n = 9$) from three experiments for one gene. Reducing sugar production levels in the apoplastic fluid were measured for *Phytophthora* XEG1 and XLP1 about 20 h in *N. benthamiana*. Each point represents the average of nine biological replicates ($n = 9$) from three experiments for one gene. Relative expression levels of total defense marker genes were assessed 24 h after infiltration using qRT-PCR. Each point represents the average of seven marker genes from three biological replicates ($n = 3$) of three experiments for one gene. In the box plots, dots represent min-to-max value of individual data points, the line indicates the median, and the box boundaries indicate the 25th and 75th percentiles. Statistical significance was determined using a two-sided *t*-test. Source data are provided as a Source Data file.

significant differences in cell death (Fig. 1d). Furthermore, variations in the abilities of XEG1 and XLP1 from different *Phytophthora* species to induce cell death, trigger defense genes, and produce reducing sugars highlight the functional diversification of these genes (Supplementary Fig. 6).

Functional divergence in the ancestral nodes of XEG1 and XLP1
To elucidate the functional divergence of XEG1 and XLP1 during *Phytophthora* evolution, we reconstruct the ancestral genes of XEG1 (XEGa) and XLP1 (XLPa), as well as their common ancestor gene (XELa) using PamlX¹⁶ (Supplementary Fig. 7). We initially assessed the ability of XEGa, XLPa, and XELa to cause cell death and analyzed structural differences. Even though the cell death-inducing capacity of XEGa and XLPa was only approximately two-fifths of that of PsXEG1, both XELa, XEGa and XLPa effectively induced cell death and were expressed correctly in *N. benthamiana* (Supplementary Fig. 8b–e). Structural comparison analyses showed that common ancestor XELa shares similar overall conformations with the corresponding XEG1 and XLP1 from *P. sojae* and *Phytophthora parasitica*, respectively, with only minor differences in specific regions (Supplementary Fig. 8a, f).

To validate the functional divergence between XEG1/XLP1 and XELa during *Phytophthora* evolution, we used Cas9-mediated homologous gene replacement in *P. sojae* (P6497) to generate homozygous lines wherein PsXEG1 or PsXLP1 were replaced with XELa (T9^{XELa-PsXEG1}, T41^{XELa-PsXEG1}, T20^{XELa-PsXLP1}, and T38^{XELa-PsXLP1}) (Supplementary Fig. 9a, b). All transformants showed normal mycelium growth compared to the control (Supplementary Fig. 9c, d). Replacing PsXEG1 or PsXLP1 with XELa reduced the virulence of *P. sojae* on soybeans (Fig. 2a–c). But compared to the XEG1 or XLP1 knockout mutants, the reduced impact on the pathogenicity of replacement transformants resulted in relatively minor changes, which may be attributed to the retained hydrolytic activity of the ancestral genes (Supplementary Fig. 9e). These results confirmed the functional divergence of XELa after its initial generation.

To delineate the divergence of XEG1 and XLP1 in *Phytophthora*, we reconstructed the ancestral genes of XEG1 and XLP1 at each evolutionary node of *Phytophthora* using PamlX¹⁶. These ancestral genes were subsequently synthesized and efficiently expressed in *N. benthamiana*, as confirmed using western blot (Supplementary Fig. 10a, d). We then examined the capacity of them to trigger cell

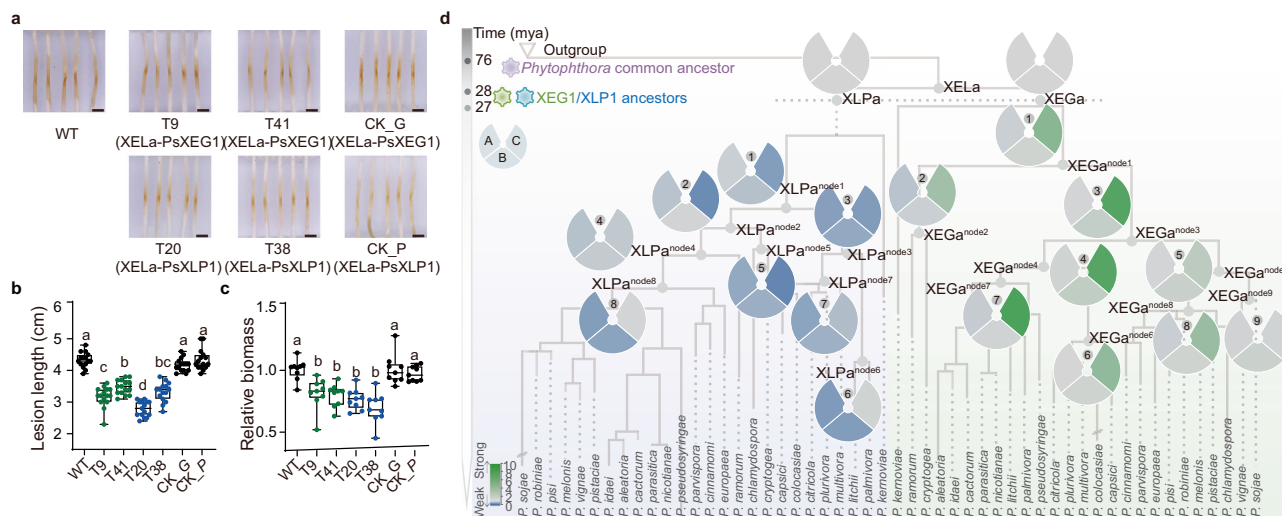


Fig. 2 | A distinct function for the ancestral variant of the XEG1 and XLP1 genes in *Phytophthora*. **a** Virulence of *P. sojae* transformants on soybean hypocotyls. Representative symptoms at 48 h post-inoculation (hpi). The transformants include *XELa* replacing *PsXEG1* (T9, T41, and control, CK_G) and *XELa* replacing *PsXLP1* (T20, T38, and control, CK_P). Experiments were repeated three independent times with similar results. **b**, **c** Impact of *PsXEG1* or *PsXLP1* replacement on virulence in etiolated soybean hypocotyls. **b** Lesion lengths on hypocotyls produced by *P. sojae* ($n = 15$). **c** Relative biomass of the wild-type and transgenic *P. sojae* mutants infecting etiolated soybean hypocotyls, measured by gDNA qPCR ($n = 9$). **b**, **c** In the box plots, dots represent min-to-max value of individual data points, the line indicates the median, and the box boundaries indicate the 25th and 75th percentiles. Three independent experiments obtained similar results. Pairwise significance was determined using Duncan's multiple range test ($p < 0.01$), with different letters representing significant differences. **d** Comparison of different ancestral nodes of *Phytophthora* XEG1 and XLP1 regarding their ability to induce cell death, produce

reducing sugar, and their relative expression of defense genes. The age of the common ancestor proteins in millions of years is indicated at the corresponding node. The background shows a maximum likelihood evolutionary tree used to reconstruct ancestral genes, with the outgroup and partial terminal genes combined and nodes labeled accordingly. The pie chart illustrates the variations in activity efficiency, with green indicating an increase and blue indicating a decrease in the evolutionary pathways. At each ancestral node, the pie represents the average fold change in phenotypic measures normalized to XEGa or XLPa, respectively: reducing sugar (A), electrolyte leakage (B), and the relative expression of defense genes (C), including *Pti5*, *Acre31*, *CYP71D20*, and *PAL10*. The bottom pie chart corresponds to electrolyte leakage ($n = 9$ biological replicates), the right pie to the relative expression of defense genes ($n = 3$ biological replicates), and the left pie to reducing sugar production levels ($n = 9$ biological replicates). Source data are provided as a Source Data file.

death, induce defense gene expression, and produce reducing sugars via *Agrobacterium*-mediated transient expression. Consistent with the XLP1 decoy model, the XLP1 subclade showed a considerable decline in the capacity of ancestral nodes to induce defense marker genes *Pti5*, *Acre31*, *CYP71D20*, or *PAL10* expression and production of reducing sugar. While the XEG1 subclade showed upregulation in immunity, the process of producing reducing sugar did not show a clear pattern (Fig. 2d).

To investigate these differing patterns, we compared the protein sequences and analyzed¹⁷ the correlation between amino acid site variation and their associated phenotypes. Each clade exhibited a preference for mutations at specific amino acid sites. The XEG1 subclade showed mutations at sites 20, 31, 32, and 58, while the XLP1 subclade displayed mutations at sites 27, 28, 33, 88, 91, and 120 (Supplementary Fig. 10a). A correlation heatmap of these variant sites and phenotypic changes revealed that certain sites were closely related to specific phenotypes. Specifically, sites 31, 91, and 120 were linked to enhanced phenotype traits in the XEG1 subclade, while sites 20, 27, 28, 33, and 58 were associated with reduced phenotype traits in the XLP1 subclade (Supplementary Fig. 10b). Furthermore, synergistic effects between different amino acid sites were observed (Supplementary Fig. 10c). These findings suggest that the critical role of amino acid site variations in driving the functional differentiation of *Phytophthora* XEG1 and XLP1.

Roles of selection pressure sites of XEG1/XLP1 in *Phytophthora* host ranges

To evaluate the selection pressure sites in XEG1 and XLP1 following the formation of *Phytophthora*, we employed the MEME (Mixed Effects Model of Evolution)^{18,19} to analyze the nonsynonymous and

synonymous substitution rate ratio (ω) and conducted significance testing for the ω values across all analyzed XLP1 and XEG1. The results identified 14 positive selection sites in the XEG1/XLP1 gene pair, visualized through an amino acid logo (Supplementary Fig. 11a). Considering previous studies demonstrating that XEG1 is subjected to three layers of host defense, including inhibitors (GmGPI1), proteases (GmAP5), and receptors (RXEG1)^{12–14,20}, we analyzed the overlap between the binding sites of these host defense molecules and the positive selection sites within the XEG1/XLP1 gene pair. Apart from amino acid residue W at position 28, nearly all positive selection sites do not overlap with the binding sites of GmGPI1, GmAP5, or RXEG1. This suggests that the divergence in positive selection sites may be driven by other evolutionary factors (Supplementary Fig. 11a).

To determine whether positive selection sites simply reflect the general genotypic relationship between species, we conducted a hypothesis-driven analysis. We hypothesized that if positive selection sites were indicative of general genotypic relationships, species-specific characteristics would manifest as shared differentiating sites in the XEG1/XLP1 sequences of each *Phytophthora* species when compared to other *Phytophthora* XEG1/XLP1 sequences. To test this hypothesis, we selected *P. capsici* and performed pairwise comparisons of their XEG1/XLP1 sequences with those from other *Phytophthora* species (Supplementary Fig. 12a). The results revealed that, compared with the XEG1/XLP1 sequences of 13 other *Phytophthora* species, the shared differentiating sites among different *P. capsici* isolates showed no overlap with the positive selection sites in XEG1/XLP1 (Supplementary Fig. 12b). These findings suggest that the positive selection sites in XEG1/XLP1 are not indicative of general genotypic relationships between species but instead reflect species-specific evolutionary pressures.

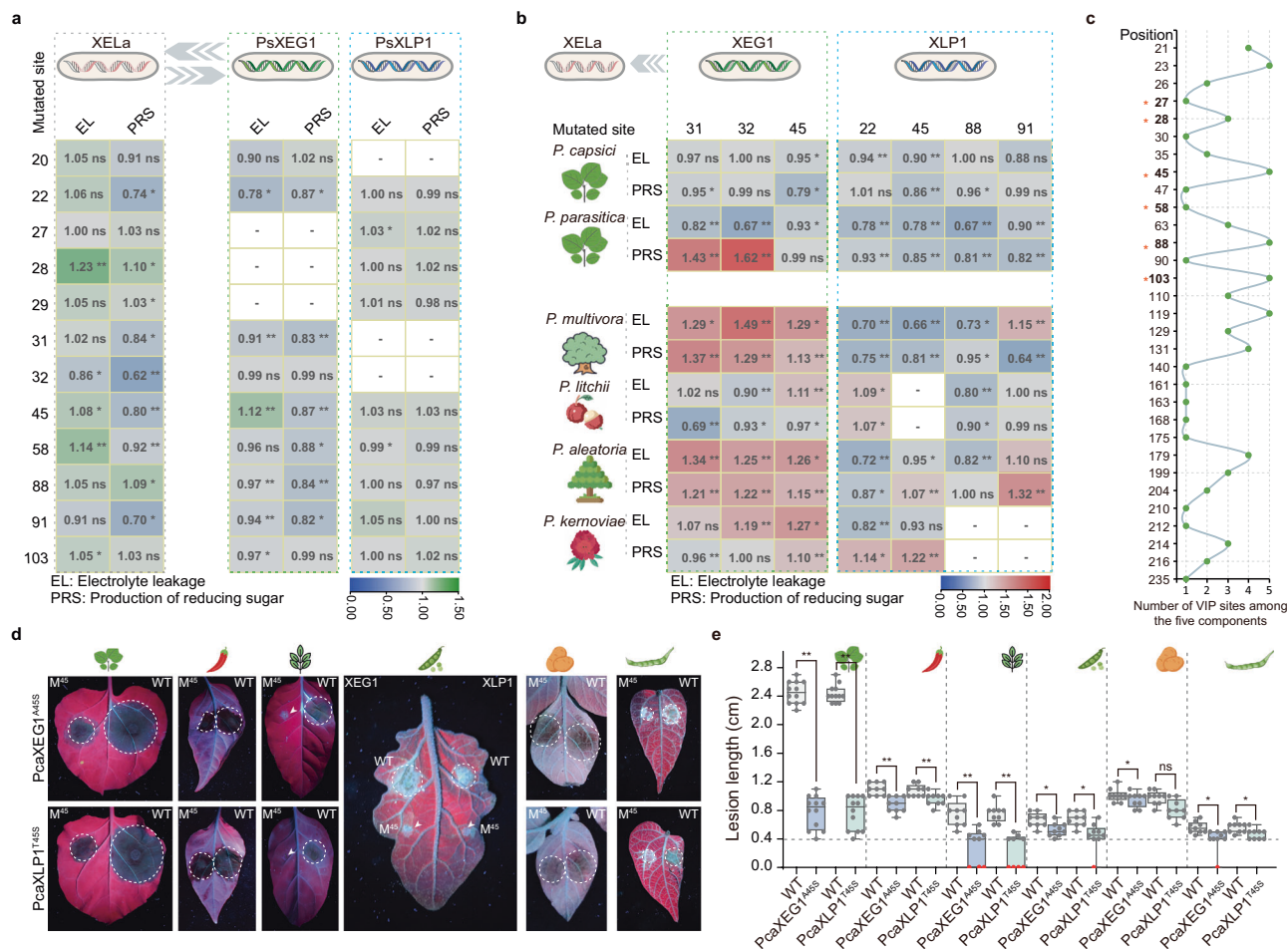


Fig. 3 | Effect of selection pressure sites on the function of XEG1 and XLP1.

a, b Mutational analysis of putative functional sites in XELa and *Phytophthora* XEG1/XLP1. Single amino acid point mutation names are indicated on the left (a) and at the top (b). Details of the mutants are in Supplementary Fig. 13. “-” means no test. “EL” means electrolyte leakage. “PRS” means production of reducing sugar. Each measurement of a mutant protein was based on the mean value, with data normalized to the wild-type proteins ($n = 9$, biological replicates). Experiments were repeated three independent times with similar results. Statistical significance was determined by a two-sided t -test ($*p (T \leq t) < 0.05$, $**p (T \leq t) < 0.001$). The green (a) and red (b) colors represent enhanced phenotypes of the mutants, blue indicates weakened phenotypes, and gray represents little to no change. Cartoons were free and downloaded from the website (<https://www.flaticon.com> or <https://icons8.com/icons>). **c** Summary of the occurrence of variable importance projection (VIP) sites at each amino acid position within the five components related to Supplementary Fig. 14. Red stars represent sites under positive selection pressure. **d** Disease symptoms of wild-type and *P. capsici* transformants. “M45” refers to the

substitution of the positive selection site at position 45 in *P. capsici* XEG1 and XLP1 (PcaXEG1 and PcaXLP1, respectively) with the ancestral amino acid. Infection of *P. capsici* transformants and wild-type on the leaves of *N. benthamiana*, pepper, *Nicotiana tabacum* (tobacco), pea, potato, and snow pea plants inoculated with mycelial plugs, respectively. The leaves were photographed under UV light. Each experiment was repeated three times with similar results. **e** Positive selection site 45 influences the expansion capabilities of *P. capsici* across different host plants. The dotted line indicates the diameter of the hyphae plugs. In the box plots, dots represent min-to-max value of individual data points ($n = 9$ and $n = 12$ for *N. benthamiana*), the line indicates the median, and the box boundaries indicate the 25th and 75th percentiles. Red dots represent almost no infection of *P. capsici*. All mutants were compared with the wild-type strains, and statistical significance was determined using a two-sided t -test ($*p (T \leq t) < 0.05$, $**p (T \leq t) < 0.001$). Each experiment was repeated three times. Source data are provided as a Source Data file.

To investigate the impact of these sites on the functional differentiation of XEG1/XLP1, we constructed the bidirectional mutants of the ancestral gene (XELa) and PsXEG1/PsXLP1 (Supplementary Fig. 11b). We determined their capacities to trigger cell death and produce reducing sugars in *N. benthamiana* using *Agrobacterium*-mediated transient expression. During the bidirectional mutation process of PsXEG1 or PsXLP1 and XELa, most of the sites were implicated in the reduction of sugar production capacity, although the PsXLP1 mutant did not exhibit any typical phenotypic changes (Fig. 3a). Following site identification and considering the differences between *Phytophthora* XEG1/XLP1 and XELa sequences, six sites were selected for further mutation analysis in other *Phytophthora* species (Supplementary Fig. 11b). These six sites significantly altered their ability to produce reducing sugar (Fig. 3b). Additionally, electrolyte

leakage data showed that mutations at positive selection pressure sites variably affected their abilities to induce cell death (Fig. 3a, b). These proteins were efficiently expressed in *N. benthamiana* (Supplementary Fig. 13). These results indicate that positive selection pressure sites are involved in the functional capacities of *Phytophthora* XEG1/XLP1.

Considering the findings by Kronmiller et al., which suggest that hydrolases may influence the host range dynamics of *Phytophthora*, we further analyzed the relationship between sequence variations in *Phytophthora* XEG1 and XLP1 and host range diversity. Following the classification system established by Kronmiller et al., we categorized *Phytophthora* species into four host range groups: narrow (confined to one plant host genus), multiple (within two to nine host genera), wide (spanning 16 to 55 host genera), and huge (spanning 107 to 327 host genera)⁸. Multivariate statistical analysis revealed that 31 amino acid

sites, identified as variable importance projection (VIP) sites, were associated with host range variation among *Phytophthora* species (Supplementary Fig. 14). Based on the frequency of these sites across five components, five amino acid sites were identified as being closely related to changes in host range. Among these, three sites (positions 45, 88, and 103) were found to be under positive selection pressure (Fig. 3c), indicating that the positive selection acting on XEG1/XLP1 in *Phytophthora* is closely correlated with their host ranges diversity (Fig. 3c and Supplementary Fig. 14).

To determine the relationship between association sites and the host range of *Phytophthora* species, we selected *Phytophthora capsici*, a species with a wide host range (infecting over 16 plant genera), for further investigation. Among the three positive selection sites previously identified as being associated with host range variation, site 45 ranked highest based on the variable importance projection (VIP) contribution (Fig. 3c and Supplementary Fig. 14). Thus, site 45 of *P. capsici* XEG1 (PcaXEG1) and *P. capsici* XLP1 (PcaXLP1) was chosen for mutation analysis. Utilizing Cas9-mediated homologous gene replacement in *P. capsici* (LT1534), we generated homozygous lines in which the alanine (A) and threonine (T) at site 45 in PcaXEG1 and PcaXLP1 were replaced with serine (S) from the ancestral gene XELa, respectively (T2, T12: PcaXEG1^{A45S}; T8, T12: PcaXLP1^{T45S}) (Supplementary Fig. 15a, b). All transformants exhibited normal mycelium growth (Supplementary Fig. 15c, d). We further conducted infection assays on *N. benthamiana*, pepper, *Nicotiana tabacum* (tobacco), pea, potato, snow pea, green bean, edamame, tomato, carrot, yellow potato, cowpea, purple lentil, and red peanut. The results showed that while the mutants exhibited no significant differences in infection capacity on green bean, edamame, tomato, carrot, yellow potato, cowpea, purple lentil, red peanut, and potato, and their pathogenicity was significantly reduced on *N. benthamiana*, pepper, tobacco, pea, and snow pea. Notably, the mutants displayed almost no expansion on tobacco and pea when comparing the inoculation plug diameter to the pathogen growth diameter (Fig. 3d, e and Supplementary Fig. 15e). These findings demonstrate that the positive selection sites in XEG1/XLP1 differentially affect *P. capsici*'s ability to infect various hosts, further suggesting that these sites contribute to the pathogen's host range.

To investigate that whether the selection pressure sites of XEG1 and XLP1 are present in natural populations of *Phytophthora* species, we analyzed the variations in the XEG1 and XLP1 across more than 128 previously documented *Phytophthora* isolates^{21–23}. Positive selection sites, including positions 20, 22, 28, 62, 88, 91, 103, and 120, were identified within these populations. However, the frequency of mutations and the specific positions of these sites varied among different *Phytophthora* species (Fig. 4a, d and Supplementary Fig. 16). Given the currently limited number of sequenced *Phytophthora* populations, some positive selection sites, such as position 45, were not detected in the existing datasets. However, these findings strongly suggest the presence of selection pressures within natural *Phytophthora* populations and indicate ongoing evolutionary forces acting on the XEG1/XLP1 gene pair.

Roles of selection pressure sites of XEG1/XLP1 in *Phytophthora* host adaptability

To investigate the impact of positive selection sites on *Phytophthora* host adaptability, in addition to the amino acid at position 45, we also selected position 31, a positive selection site that significantly impacts PsXEG1 hydrolysis activity (Fig. 3a). At position 31, serine (S) in PsXEG1 was mutated to alanine (A), and at position 45 in PsXLP1, alanine (A) was mutated to serine (S) from the ancestral gene XELa. Homozygous lines were generated using the CRISPR/Cas9 system (T10, T14: PsXEG1^{S31A}; T11, T49: PsXLP1^{A45S}) (Supplementary Fig. 17a). Compared with wild-type (WT) and control (CK) lines, the mutants PsXEG1^{S31A} and PsXLP1^{A45S} exhibited normal growth (Supplementary Fig. 17b, c). However, the pathogenicity of the mutants was reduced, as evidenced

by a decline in biomass and lesion length measurements (Fig. 4b, c). These results indicate that common driving pressure sites in *Phytophthora* contribute to host adaptability and suggest that the evolutionary changes in sequences from ancestral forms to current *Phytophthora* species have enhanced their host adaptability.

Considering the presence of natural mutations at position 62, identified as a positive selection site in the natural population of *P. sojae*, we focused on a threonine (T) to isoleucine (I) mutation in XLP1 at this site (Fig. 4d). This mutation involves a shift from a polar to a nonpolar amino acid, altering the direction of the branching chain. Additionally, in *Phytophthora kernoviae*, another mutation at position 62 introduced an arginine (R), which has a long branch chain and alters the structural charge (Supplementary Fig. 18a). To explore the functional role of position 62, we used the CRISPR/Cas9 system to mutate this position to either isoleucine (I) or arginine (R), generating transformants (T5, T7: PsXLP1^{T62I}; T14, T45: PsXLP1^{T62R}) (Supplementary Fig. 18b). Compared with wild-type (WT) and control (CK) lines, mutants PsXLP1^{T62I}, PsXLP1^{T62R} exhibited normal growth (Supplementary Fig. 18c). The pathogenicity of PsXLP1^{T62I} mutants increased significantly, whereas it declined in PsXLP1^{T62R} mutants. Biomass measurements of *P. sojae* were consistent with lesion length (Fig. 4e, f). These results indicate that *Phytophthora*'s common evolutionary pressure is present in natural populations and influence *Phytophthora*'s ability to adapt to host.

Discussion

Our results propose a model in which *Phytophthora*-specific selection pressures on XEG1 and its paralog XLP1 are closely linked to the host range diversity of *Phytophthora* beyond their roles host adaptability (Fig. 4g). Originating from horizontal gene transfer events from fungi, XEG1 underwent gene duplication, giving rise to a paralog positioned in head-to-head configuration with its counterpart^{11,13}. This gene pair has evolved into a genus-specific feature of *Phytophthora*, serving as a focal point of coevolutionary struggle in diverse *Phytophthora*-plant pathosystems. Previous research has underscored the role of XEG1 in virulence through hydrolytic activities, countered by host defenses via inhibitors, proteases, and recognition receptors^{12–14,20}. In response, *Phytophthora* utilizes strategies such as decoys, glycosylation, and other effectors to evade host defenses^{13–15}, underscoring its significance beyond its virulence-related functions. Our findings demonstrate that positive selection sites in XEG1/XLP1 are integral to the host adaptability of *Phytophthora*. The ancestral genes of XEG1/XLP1 exhibit significant sequence divergence compared to modern XEG1/XLP1, with several positive selection sites identified in these differences. Mutating these sites in *Phytophthora* XEG1/XLP1 to their ancestral counterparts resulted in reduced pathogenicity, suggesting a positive correlation between these evolutionary changes and host adaptability. Additionally, the involvement of XEG1/XLP1 in the host range diversity of *Phytophthora* further emphasizes their importance as genus-specific genes in *Phytophthora*. Beyond this, considering that some XLP1 orthologs exhibit hydrolytic activity, our results imply that XLP1 may have additional roles beyond its decoy function in *P. sojae*, potentially contributing to other essential functions in different *Phytophthora* species.

Natural selection, a fundamental mechanism of evolutionary change, drives the evolution of adaptive traits. Effectors exhibiting sequence and structural polymorphisms can elude the counter-defenses of hosts^{24,25}. Previous investigations have indicated that the XEG1/XLP1 pair experiences diverse selection pressures from host inhibitors, proteases, and receptors. However, our observations indicate that the binding sites of XEG1 or XLP1 with these three classes of host proteins do not coincide with sites subjected to selection pressure. This suggests that the XEG1/XLP1 gene pair in *Phytophthora* is under a different type of selection pressure, possibly related to the hydrolytic activity of XEG1. Despite previous in vitro enzyme activity

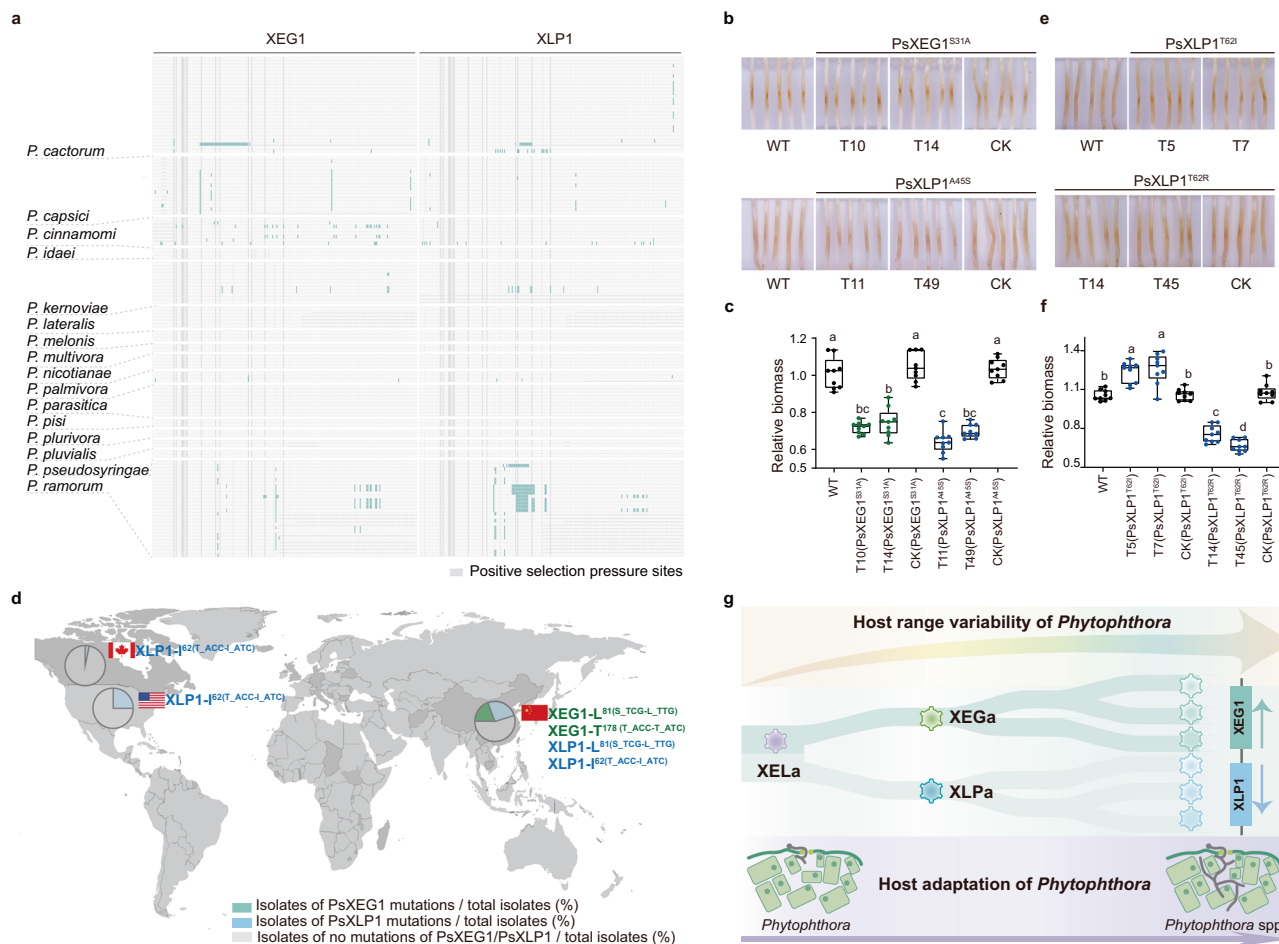


Fig. 4 | Positive selection pressure sites facilitate the adaptability of *Phytophthora sojae* to soybean. **a** Schematic comparison of various XEG1 and XLP1 mutants across multiple *Phytophthora* genomes. Each row represents a different genome, and mutation sites are highlighted in green, positive selection sites are indicated with dark gray, and missing sequences are displayed in light gray. Detailed mutation information is available in Supplementary Data 4. **b, c** Positive selection pressure sites enable the pathogenicity of *P. sojae*. **d** Natural mutation sites of *P. sojae* isolates. A map depicting the geographic distribution of *P. sojae* single nucleotide polymorphisms (SNPs). Variations in *PsXEG1* and *PsXLP1* across homozygous and heterozygous mutant SNPs are presented for each isolate. Detailed mutation information is provided in Supplementary Data 5. **e, f** Positive selection pressure site 62 in *P. sojae* population isolates enables the pathogenicity of *P. sojae*. **b, e** Representative images of disease symptoms were photographed at

48 hpi. **c, f** Relative biomass of mutant strains and wild-type at 48 hpi was quantified using genomic DNA qPCR. In the box plots, dots represent min-to-max value of individual data points ($n = 9$ biological replicates), the line indicates the median, and the box boundaries indicate the 25th and 75th percentiles. Statistical differences were assessed using Duncan's multiple range test, with different letters indicating significant differences ($p < 0.01$). Source data are provided as a Source Data file. **g** Model: XEG1 and XLP1 originated within the *Phytophthora* genus. Over time, evolutionary differentiation within the genus led to the development of XEG1 and XLP1 from ancestral genes across various *Phytophthora* species. Genus-specific selection pressures acting on the XEG1/XLP1 gene pair have been pivotal for host adaptation and are strongly associated with the variability of *Phytophthora* host ranges.

studies showing that XEG1/XLP1 can hydrolyze xyloglucan, its degradation substrates in host plants require further study. Additionally, this widespread selection pressure in natural *Phytophthora* populations implies the persistence of this driving force.

Dynamic changes in the host range of *Phytophthora* are likely influenced by multiple factors beyond the genetic evolution of specific genes. Human activities play a significant role in the long-distance dispersal of plant pathogens, facilitating the introduction of *Phytophthora* species into new regions and affecting host adaptability. For instance, the global nursery trade has contributed to the emergence of new hosts for *P. ramorum*²⁶. In addition, *P. ramorum* and *P. kernoviae* have been found on hikers' boots in infested areas, underscoring the role of human-mediated dispersal in spreading these pathogens^{27–29}. Understanding the geographic origins of invading *Phytophthora* species, their evolutionary trajectories, and potential sources of migration will require more extensive genomic data, making this an important direction for future research.

The host range dynamics of *Phytophthora* are further influenced by the functional diversity of apoplastic effectors. Apoplastic effectors of *Phytophthora* encompass various proteins such as glycoside hydrolases, protease inhibitors, necrosis-inducing proteins (NLPs), proteases, lipases, and lipid-binding proteins⁸. The protease inhibitor EPIC1 of *Phytophthora mirabilis* is involved in the transition from the four o'clock flower to potato hosts. This study further suggests the role of apoplastic effectors in the host range dynamics of *Phytophthora*³⁰. Host availability alone does not solely dictate oomycete diversification⁴. The evolutionary trajectory of pathogens may have been influenced by environmental changes or facilitated through horizontal gene transfer events from fungi^{9,31}, bacteria³², and animals³³. A comparative genomic analysis involving 31 *Phytophthora* genomes identified 44 horizontal candidates, who are also associated with enzymes involved in plant cell wall deconstruction, evasion, and protection from host defenses⁸, including XEG1¹¹. Although this study suggests that XEG1/XLP1 may contribute to alterations in the host

range of *Phytophthora*, XEG1/XLP1 does not represent the sole determinant, warranting further investigation into additional genes and factors.

Methods

Plant and microbe growth conditions

Nicotiana benthamiana, *Nicotiana tabacum*, and other plants were grown in vermiculite in a greenhouse at 25 °C under a 16-h light/8-h dark cycle. The etiolated soybean cultivar Hefeng 47, susceptible to *Phytophthora sojae* strain P6497, was grown in the dark for 4 days at 25 °C in vermiculite.

Agrobacterium tumefaciens and *Escherichia coli* strains were cultured on Luria-Bertani (LB) agar at 28 °C and 37 °C, respectively. *P. sojae* (P6497) and *Phytophthora capsici* (LT1534) were cultured on 10% (v/v) V8 medium at 25 °C in the dark.

Plasmid construction

Plasmids are often constructed according to standard molecular engineering procedures. Part of the *Phytophthora* XEG1 and XLP1 genes, as well as the ancestral genes constructed in the Pbin-3 × HA vector, were synthesized depending on predicted introns, as listed in Supplementary Data 2 and 6 (Generalbiol, Chuzhou, China). Single guide RNAs (sgRNAs) targeting *PsXEG1*, *PsXLP1*, *PcaXEG1*, and *PcaXLP1* genes were constructed in the plasmid pYF515. Homologous recombination plasmids for ancestral replacement or single amino acid mutations, each flanked by 1 kb of homology arms, were constructed in the PVX-3 × HA vector.

Proteome database search and sequence analysis

Proteome data from Supplementary Data 1 were used for Hidden Markov Model (HMM) searches against the conserved Glycohydro 12 domain (PFAM ID: PF01670). Non-redundant protein sequences were retrieved and analyzed for protein domains and signal peptides using SMART (<http://smart.embl-heidelberg.de>) and SignalP 6.0 (<http://www.cbs.dtu.dk/services/SignalP-6.0>). Enzyme sites within GH12 proteins were predicted using Conserved Domains (<https://www.ncbi.nlm.nih.gov/Structure/cdd/wrpsb.cgi>).

Genomic DNA (gDNA) used for collinearity analysis, as well as cDNA sequences for experimental analysis, were validated against current RNA-sequencing data and protein annotation files (GFF). Any regions with potential annotation errors or lacking RNA-seq reads from the Sequence Read Archive were manually reannotated based on genomic data and listed in Supplementary Data 2.

Collinearity analyses were performed using the One-step MCSanX module in TBtools (v2.067), which generated the “. collinearity”, “. gff”, and “dualSynteny.ctl” files. Due to low-quality genome assemblies, the orthologs of *PsXEG1* and *PsXLP1* were located on separate contigs in nine *Phytophthora* species, complicating the identification of these as genuine genes or pseudogenes. In six species, only a single XEG1 or XLP1 was found, and paired gene relationships could not be determined. Upstream and downstream regions of *XEG1* orthologs were highlighted, and dual synteny plots were created for visualization.

For natural mutation analysis in *Phytophthora* isolates (Fig. 4a, d), reference protein sequences from Supplementary Data 2 were used to query each isolate’s translated nucleotide database via NCBI’s tblastn. More details are listed in Supplementary Data 4 and 5.

Phylogenetic analysis

The phylogenetic tree of oomycete species: OrthoFinder v2.3.12 (<https://github.com/davidemms/OrthoFinder/releases>) was used to find orthogroups and orthologs, use the multiple sequence alignment species tree method (-M msa), infer a rooted species tree for the species being analyzed, and map the gene duplication events from the

gene trees to branches in the species tree. Hosts of pathogens cited by Wikipedia and references listed in Supplementary Data 1. Cartoons were free and downloaded from the website (<https://www.flaticon.com> or <https://icons8.com/icons>). The phylogenetic tree used to estimate the time when ancestral genes began to diverge also used the same method in Orthofinder.

Phylogenetic analysis of all GH12 proteins and used to calculate selection pressure for XEG1 and XLP1 subclades were performed using an approximate maximum likelihood method implemented in IQ-Tree v1.6.12. All the trees were assessed with 1000 bootstraps, displayed using iTOL v6 (<http://itol.embl.de>).

TimeTree (Fig. 2d) analysis was conducted using the Reltime method and the JTT matrix-based model in MEGA7, with the input of 28 concatenated amino acid sequences generated by OrthoFinder v2.3.12. OrthoFinder v2.3.12 was used to identify orthogroups and orthologs, with parameters “-M msa” for gene tree inference and the STAG algorithm for rooted species tree inference. The divergence node time between *Phytophthora cinnamomi* and *P. sojae* was fixed, setting the maximum divergence time at 10.2 and the minimum divergence time at 9.9.

Conservation analysis

Evolutionary conservation of amino acid positions in XEG1/XLP1 orthologs was assessed using the ConSurf server (<https://consurf.tau.ac.il>). Based on ConSurf conservation scores, the conservation patterns of XEG1 and XLP1 clades were visualized on 3D structures modeled from PDB: 7w3v (chain A) using PyMOL (<https://pymol.org/edu/>). The 3D structures of *PsXLP1*, *PpXEG1*, *PpXLP1*, and ancestral proteins were predicted using AlphaFold2 via ColabFold v1.5.5 (<https://colab.research.google.com/github/sokrypton/ColabFold/blob/main/AlphaFold2.ipynb#scrollTo=G4yBrceufbf3>). Structural alignment for comparison was performed using the pair-fit method in PyMOL (version 2.5.2). Weblogo 3 (<https://weblogo.threepiusone.com/create.cgi>) was used to create logo plots showing conserved sites in proteins with intact domain organizations.

Selection pressure analysis of XEG1/XLP1 clades

Selection pressure was analyzed using the CODEML module in PAML v4.9j, which employs two branching models to calculate the dN/dS ratio³⁴. Phylogenetic trees were constructed based on protein alignments using the maximum likelihood method in IQ-Tree v1.6.12, and tree files were generated (.tree). The cDNA sequences of coding regions (codons 1 to 723) were aligned using ClustalW in MEGA7, followed by manual gap removal, and the resulting files were converted to the “.nuc” format. Selection pressure was assessed by editing the.ctl file and analyzing in PAML v4.9j. Branches corresponding to the XEG1 and XLP1 clades were labeled as “\$1” and “\$2,” respectively. One outgroup used by all fungi, oomycetes, and bacteria, and another outgroup used by the *Phytophthora* GH12 family proteins, where XEG1 and XLP1 were paired. For model comparison, we obtained lnL1 = -107,588.8137 and lnL0 = -107,601.6545, with a pchisq value of 2.65E -06 (5% significance level, Supplementary Fig. 2a). Similarly, we obtained lnL1 = -55,764.8344 and lnL0 = -55,774.1569, with a pchisq value of 8.94E -05 (5% significance level, Fig. 1c).

Reconstruction of ancestral XEG1/XLP1 proteins sequences

Protein sequences corresponding to the hypothetical ancestors of the *Phytophthora* XEG1/XLP1 pairs were inferred using the CODEML program in package pamlX. A total of 52 sequences of XEG1/XLP1 pairs and 3 nearest outgroup proteins were used in the prediction. Amino acid sequences of coding regions were aligned using ClustalW, with gaps removed based on the *PsXEG1* sequence (codons 1-241), resulting in a new alignment file (.pml). Phylogenetic trees were constructed using the maximum likelihood method in MEGA7, and the resulting tree file

(tree) was generated. Ancestral sequences were predicted using the CODEML program with the alignment, amino acid rate file ("wag.dat"), and model 3 (Empirical+F).

Selection pressure sites analysis of *Phytophthora* XEG1/XLP1

Selection sites were analyzed using the MEME method (Maximum Likelihood Estimation of Evolutionary Models) within the HyPhy 2.5.48 software package. This method identifies amino acid positions evolving faster than expected under a neutral model, indicating positive selection. A total of 52 XEG1/XLP1 coding region sequences were aligned using ClustalW in MEGA7 and generated new alignment file. Phylogenetic trees were constructed using the maximum likelihood method in MEGA7, and the 'foreground' branches were marked on the PhyloTree website (<https://phyloree.hyphy.org/>) to update the phylogenetic tree. To assess the statistical significance of ω , likelihood ratio tests (LRTs) were performed, comparing a neutral model (no selection) and a selection model. Sites with $\omega > 1$ and a significant p value of 0.05 were identified as under positive selection pressure.

Agrobacterium tumefaciens infiltration

We transformed verified plasmids with the strain GV3101 and cultured them on liquid medium (LB) with antibiotics at 28 °C for 36 h. We resuspended the *Agrobacterium* in infiltration buffer (10 mM MgCl₂, 200 mM acetosyringone, 10 mM MES, pH 5.7) after identifying the correct clone. The phenotypes of cell death induced by XELa, XEGa, XLPa, PpXEG1, PpXLP1, and PsXEG1 were early and strong, in order to compare the differences, the final concentration of OD₆₀₀ = 0.2 was chosen. For the other electrolyte leakage measurement experiments, the defense marker gene induction experiments, the reducing sugar production experiments, and the protein extraction triggered by various *Phytophthora* XEG1 and XLP1, different ancestral node proteins, and mutational sites in XELa and *Phytophthora* XEG1/XLP1, the final concentration for each strain in the infiltration medium was diluted to OD₆₀₀ = 0.4. Each gene or mutant was injected on the leaves, avoiding the veins.

Electrolyte leakage assay

To identify the ability of different *Phytophthora* XEG1 and XLP1 to induce cell death, we performed measurements at 48 h. In order to distinguish the influence of site mutation differences, we measured experiments at about 30 h. XELa, XEGa, XLPa, PpXEG1, PpXLP1, PsXEG1 inducing cell death were measured more earlier at about 28 h, when the leaves were not completely necrotic. For cell death, we performed a point injection into an area of approximately more than 1 cm in diameter, and marked.

Five 1 cm leaf discs were cut after infiltration and floated in 5-mL Ep tubes containing deionized water for three hours at room temperature. Measurements were made of the first electrolyte leakage levels. After boiling for 10 min and cooling to room temperature, the final electrolyte leakage values were determined. A conductivity meter was used to measure the electrolyte leakage values (Con 700; Consort, Turnhout, Belgium). Electrolyte leakage was measured by dividing the second value by the first value and multiplying by 100.

Production of reducing sugar assays

The apoplastic fluid (AF) in *N. benthamiana* leaves was isolated 20 h after infiltration in *N. benthamiana*. Inject approximately 3–4 circles per leaf. Five 2.5-cm leaf discs were cut and floated in 25-mL Ep tubes containing 1 × PBS. After pumping for 2 min for each timer with the vacuum pump, slowly open the air valve. Use absorbent paper to carefully dry the buffer on the surface of the leaf discs and place them in the centrifuge device. Centrifuge at 1500 × g for 10 min. Ten μ L of AF was transferred into PCR tubes, including 100 μ L of DNS solution (DNS, D7800; Solarbio) and 90 μ L of distilled water. Incubate the tubes at 37 °C for 30 min, then heat them at 99.9 °C for 10 min. Measure them

with a SpectraMax® M5 microplate reader at 540 nm. The standard curve was measured with 0, 0.2, 0.4, 0.6, 0.8, and 1 mg/L standard of D-glucose solution (Sangon) in Na-acetate buffer (0.05 M, pH 5.5), which had been Milli-Q filtered.

Immunoprecipitation and western blotting

Protein extractions and immunoblots were performed as previously described¹³. Antibodies used: Anti-HA (Mouse Antibody, 1:5000 dilution, Abmart, lot#324184), R dye 800CW Goat anti-Mouse IgG(H + L) antibody(926-32210, LI-COR, 1:10,000).

Whole genome resequencing data analysis

The adapter low-quality reads were filtered using Trim Galore. The Burrows-Wheeler Transform Alignment (BWA) v0.7.5a was then used to mapped clean reads to the *P. sojae* reference genome v3.0. The Samtools software package v1.8 was used to sort and convert mapped bam files. We used IGV v2.16.1 to view the ".bam" files and count the PsXEG1 and PsXLP1 mutations. More details are listed in Supplementary Data 5.

Statistics and reproducibility

Samples were allocated randomly into experimental groups. Samples sizes were determined based on the generation of convincing and compelling results. Investigators were blinded to the experiments and assays. At least three biological replicates were performed in all experiments. The number of replicates is indicated in the figure legend. Data were analyzed using boxplots created with Graphpad Prism version 8.0 software (<https://www.graphpad.com/>). Whiskers mean "min to max, and show all points". In the box plots, dots represent the min-to-max value of all individual data points, the line indicates the median, and the box boundaries indicate the upper (25th percentile) and lower (75th percentile) quartiles. For data exclusions, only analysis of mutations in natural population isolates of *P. sojae*. The sequence reads with low quality are more likely derived from sequencing errors, and were thus excluded. To reduce the effect of sequencing error on assembly, we performed the quality control of raw data using Trimmomatic (v. 0.38).

The normal heatmaps were constructed and visualized using TBtools (v2.067). The heatmaps in Supplementary Fig. 10 were created with MetaboAnalyst 6.0. For converting the ancestral sequence changes of the XEG1 clade compared to XEGa and the XLP1 clade compared to XLPa into binary formats. Taking the change of amino acid at site 20 as an example, the "G-G" code is 0000001, and the "A-A" code is 0000010. Taking the change in the site 90 amino acid as an example, in the XEG1 clade, the unchanged "T-T" code is 0001111, and the changed "T-S" code is 0010000. In the XLP1 clade, the unchanged "S-S" code is 0001101, and the changed "S-T" code is 0100000. Encode the dynamically changing amino acids of all ancestor nodes into binary format. At the same time, the phenotype is divided into five levels, enhanced is set to 5, weakly enhanced is set to 4, unchanged is set to 3, weakly weakened is set to 2, and weakened is set to 1. Then use MetaboAnalyst 6.0 for analysis; no sample normalization was set.

Partial least squares discriminant analysis (PLS-DA) analysis was used the 'AlignO' module in Biopython v1.75 to handle multiple sequence alignment (MSA) convert into binary format files. We labeled the host ranges set for different *Phytophthora* pathogens and analyzed with MetaboAnalyst 6.0. The PLS regression is performed using the pls function provided by R pls package. The classification and cross-validation are performed using the corresponding wrapper function offered by the caret package. Sample normalization was normalized by median, data transformation and data scaling were used the default value. Select maximum components to search is 5, cross-validation (CV) method is 5-fold CV, and performance measure is Q2. Permutation test statistic was selected separation distance (B/W), and set permutation numbers 1000, empirical p value was 0.003.

P. sojae and *P. capsici* transformation

The CRISPR-mediated gene replacement technique was used to produce homologous gene replacement mutants^{13,35}.

P. sojae growth and virulence assays

The steps are similar to those reported in the previous article¹³.

P. capsici growth and virulence assays

WT and all transformants of *P. capsici* were cultured on 10% V8 medium at 25 °C in the dark. After 4–5 days, we examined the colony diameters on the V8 medium. Mycelial plugs were infected on half of the plant leaves, and the inoculated leaves were placed in a plastic box with high humidity, the size of the lesions on the inoculated leaves was measured under UV light.

Reporting summary

Further information on research design is available in the Nature Portfolio Reporting Summary linked to this article.

Data availability

The data generated in this study are provided in the Supplementary Information/Source Data file. The PDB code for the plant receptor like protein RXEG1 in complex with xyloglucanase XEG1 structure: 7W3V. The detailed SRA project of NCBI data cited in the article also can be found at Supplementary Data. Source data are provided with this paper.

References

- Gunderson, J. H., Elwood, H., Ingold, A., Kindle, K. & Sogin, M. L. Phylogenetic relationships between chlorophytes, chrysophytes, and oomycetes. *Proc. Natl Acad. Sci. USA* **84**, 5823–5827 (1987).
- Jiang, R. H. & Tyler, B. M. Mechanisms and evolution of virulence in oomycetes. *Annu. Rev. Phytopathol.* **50**, 295–318 (2012).
- Thines, M. Phylogeny and evolution of plant pathogenic oomycetes—a global overview. *Eur. J. Plant Pathol.* **138**, 431–447 (2014).
- Matari, N. H. & Blair, J. E. A multilocus timescale for oomycete evolution estimated under three distinct molecular clock models. *BMC Evol. Biol.* **14**, 1–11 (2014).
- Haas, B. J. et al. Genome sequence and analysis of the Irish potato famine pathogen *Phytophthora infestans*. *Nature* **461**, 393–398 (2009).
- Yang, X., Tyler, B. M. & Hong, C. An expanded phylogeny for the genus *Phytophthora*. *IMA Fungus* **8**, 355–384 (2017).
- Lo Presti, L. et al. Fungal effectors and plant susceptibility. *Annu. Rev. Plant Biol.* **66**, 513–545 (2015).
- Kronmiller, B. A. et al. Comparative genomic analysis of 31 *Phytophthora* genomes reveals genome plasticity and horizontal gene transfer. *Mol. Plant Microbe Interact.* **36**, 26–46 (2023).
- Thomma, B. P., Nürnberger, T. & Joosten, M. H. Of PAMPs and effectors: the blurred PTI-ETI dichotomy. *Plant Cell* **23**, 4–15 (2011).
- Jones, J. D. G., Staskawicz, B. J. & Dangl, J. L. The plant immune system: from discovery to deployment. *Cell* **187**, 2095–2116 (2024).
- Richards, T. A. et al. Horizontal gene transfer facilitated the evolution of plant parasitic mechanisms in the oomycetes. *Proc. Natl Acad. Sci. USA* **108**, 15258–15263 (2011).
- Ma, M. Z. et al. A *Phytophthora sojae* glycoside hydrolase 12 protein is a major virulence factor during soybean infection and is recognized as a PAMP. *Plant Cell* **27**, 2057–2072 (2015).
- Ma, Z. et al. A paralogous decoy protects *Phytophthora sojae* apoplastic effector PsXEG1 from a host inhibitor. *Science* **355**, 710–714 (2017).
- Xia, Y. et al. N-glycosylation shields *Phytophthora sojae* apoplastic effector PsXEG1 from a specific host aspartic protease. *Proc. Natl Acad. Sci. USA* **117**, 27685–27693 (2020).
- Wang, Q. et al. Transcriptional programming and functional interactions within the *Phytophthora sojae* RXLR effector repertoire. *Plant Cell* **23**, 2064–2086 (2011).
- Xu, B. & Yang, Z. PAMLX: a graphical user interface for PAML. *Mol. Biol. Evol.* **30**, 2723–2724 (2013).
- Pang, Z. et al. MetaboAnalyst 6.0: towards a unified platform for metabolomics data processing, analysis and interpretation. *Nucleic Acids Res.* **52**, gkae253 (2024).
- Kosakovsky Pond, S. L. & Frost, S. D. Not so different after all: a comparison of methods for detecting amino acid sites under selection. *Mol. Biol. Evol.* **22**, 1208–1222 (2005).
- Pond, S. L. K., Frost, S. D. & Muse, S. V. HyPhy: hypothesis testing using phylogenies. *Bioinformatics* **21**, 676–679 (2005).
- Sun, Y. et al. Plant receptor-like protein activation by a microbial glycoside hydrolase. *Nature* **610**, 335–342 (2022).
- Mandal, K., Dutta, S., Upadhyay, A., Panda, A. & Tripathy, S. Comparative genome analysis across 128 *Phytophthora* isolates reveal species-specific microsatellite distribution and localized evolution of compartmentalized genomes. *Front. Microbiol.* **13**, 806398 (2022).
- Zhang, X. et al. Whole genome re-sequencing reveals natural variation and adaptive evolution of *Phytophthora sojae*. *Front. Microbiol.* **10**, 2792 (2019).
- Arsenault-Labrecque, G. et al. Stable predictive markers for *Phytophthora sojae* avirulence genes that impair infection of soybean uncovered by whole genome sequencing of 31 isolates. *BMC Biol.* **16**, 1–16 (2018).
- Attah, V. et al. Duplication and neofunctionalization of a horizontally transferred xyloglucanase as a facet of the Red Queen coevolutionary dynamic. *Proc. Natl Acad. Sci. USA* **121**, e2218927121 (2024).
- Cao, Y. et al. Structural polymorphisms within a common powdery mildew effector scaffold as a driver of coevolution with cereal immune receptors. *Proc. Natl Acad. Sci. USA* **120**, e2307604120 (2023).
- Grünwald, N. J., LeBoldus, J. M. & Hamelin, R. C. Ecology and evolution of the sudden oak death pathogen *Phytophthora ramorum*. *Annu. Rev. Phytopathol.* **57**, 301–321 (2019).
- Webber, J. F. & Rose, J. Dissemination of aerial and root infecting *Phytophthoras* by human vectors. *Proc. Sudden Oak Death Third Sci. Symp.* 195–198, <https://research.fs.usda.gov/treesearch/29882> (2008).
- Frankel, S. J., Kliejunas, J. T. & Palmieri, K. M. *Proceedings of the Sudden Oak Death Third Science Symposium*. General Technical Report PSW-GTR-214 491, 214 (US Department of Agriculture, Forest Service, 2008).
- Mullett, M. S. et al. Phylogeography and population structure of the global, wide host-range hybrid pathogen *Phytophthora × cambivora*. *IMA Fungus* **14**, 4 (2023).
- Dong, S. et al. Effector specialization in a lineage of the Irish potato famine pathogen. *Science* **343**, 552–555 (2014).
- Misner, I., Blouin, N., Leonard, G., Richards, T. A. & Lane, C. E. The secreted proteins of *Achlya hypogyna* and *Thraustotheca clavata* identify the ancestral oomycete secretome and reveal gene acquisitions by horizontal gene transfer. *Genome Biol. Evol.* **7**, 120–135 (2015).
- Belbahri, L., Calmin, G., Mauch, F. & Andersson, J. O. Evolution of the cutinase gene family: evidence for lateral gene transfer of a candidate *Phytophthora* virulence factor. *Gene* **408**, 1–8 (2008).
- Lévesque, C. A. et al. Genome sequence of the necrotrophic plant pathogen *Pythium ultimum* reveals original pathogenicity mechanisms and effector repertoire. *Genome Biol.* **11**, 1–22 (2010).
- Yang, Z. PAML 4: phylogenetic analysis by maximum likelihood. *Mol. Biol. Evol.* **24**, 1586–1591 (2007).

35. Fang, Y. & Tyler, B. M. Efficient disruption and replacement of an effector gene in the oomycete *Phytophthora sojae* using CRISPR/Cas9. *Mol. Plant Pathol.* **17**, 127–139 (2016).

Acknowledgements

We thank Prof. M. Wang (Nanjing Agricultural University), Prof. K. Duan (Nanjing Agricultural University) for insightful discussions and constructive suggestions. This research was supported by grants from the National Key Research and Development Program of China (2022YFF1001500, Y.W.), National Natural Science Foundation of China Outstanding Youth Fund (Overseas, Z.M.), Jiangsu Province Distinguished Professor (Special Support, Z.M.) and National Natural Science Foundation of China (32102172, Y.X.). Bioinformatic workstation was supported from the Bioinformatics Center, Nanjing Agricultural University.

Author contributions

W.-Y.C. and M.-Z.C. administrate the project. W.-Y.C., M.-Z.C. and Z.Q. conceived the idea, guided the project, and wrote the manuscript with feedbacks from other authors. Z.Q., C.X., C.B., J.-L.Y., Y.-H.X., M.J., Z.-X.Y., W.-X.Y., L.-H.S., L.-S.Z., W.-K.X., J.-H.B., X.-J.H., S.-H.D., Z.-Z.C., Q.M., C.H. and X.-Y.Q. performed experiments and analyzed the results. D.-S.M., Y.-W.W. and W.Y. provided advice and reagents and discussed the results.

Competing interests

The authors declare no competing interests.

Additional information

Supplementary information The online version contains supplementary material available at <https://doi.org/10.1038/s41467-025-58770-x>.

Correspondence and requests for materials should be addressed to Zhenchuan Ma or Yuanchao Wang.

Peer review information *Nature Communications* thanks Stefan Kusch and the other, anonymous, reviewers for their contribution to the peer review of this work. A peer review file is available.

Reprints and permissions information is available at <http://www.nature.com/reprints>

Publisher's note Springer Nature remains neutral with regard to jurisdictional claims in published maps and institutional affiliations.

Open Access This article is licensed under a Creative Commons Attribution-NonCommercial-NoDerivatives 4.0 International License, which permits any non-commercial use, sharing, distribution and reproduction in any medium or format, as long as you give appropriate credit to the original author(s) and the source, provide a link to the Creative Commons licence, and indicate if you modified the licensed material. You do not have permission under this licence to share adapted material derived from this article or parts of it. The images or other third party material in this article are included in the article's Creative Commons licence, unless indicated otherwise in a credit line to the material. If material is not included in the article's Creative Commons licence and your intended use is not permitted by statutory regulation or exceeds the permitted use, you will need to obtain permission directly from the copyright holder. To view a copy of this licence, visit <http://creativecommons.org/licenses/by-nc-nd/4.0/>.

© The Author(s) 2025